Zeeman interaction and Jahn-Teller effect in the Γ_8 multiplet

Naoya Iwahara, Veacheslav Vieru, Liviu Ungur, and Liviu F. Chibotaru*
Theory of Nanomaterials Group, University of Leuven, Celestijnenlaan 200F, B-3001 Leuven, Belgium
(Received 11 June 2017; published 11 August 2017)

We present a thorough analysis of the interplay of magnetic moment and the Jahn-Teller effect in the Γ_8 cubic multiplet. We find that in the presence of the dynamical Jahn-Teller effect, the Zeeman interaction remains isotropic, whereas the g and G factors can change their signs. The static Jahn-Teller distortion also can change the sign of these g factors as well as the nature of the magnetic anisotropy. Combining the theory with state-of-the-art *ab initio* calculations, we analyzed the magnetic properties of Np^{4+} and Ir^{4+} impurity ions in a cubic environment. The calculated g factors of the Np^{4+} impurity agree well with experimental data. The *ab initio* calculation predicts a strong Jahn-Teller effect in Ir^{4+} ion in the cubic environment and the strong vibronic reduction of g and G factors.

DOI: 10.1103/PhysRevB.96.064416

I. INTRODUCTION

Magnetic complexes and insulators containing heavy-transition-metal, lanthanide, or actinide ions attract significant interest because they often show single-molecule magnet behavior [1,2] and various exotic magnetic phases [3–5]. In these phenomena, local magnetic anisotropy with unquenched orbital angular momentum plays a key role. Particularly, the magnetic interactions such as Zeeman interaction [6] and exchange interaction [7,8] become of tensorial type with the increase in the numbers of electronic states which are relevant to the magnetism. At the same time, the vibronic coupling between the (quasi)degenerate electronic states and the lattice vibration [9–11] leads to a more complex nature of the ground states. Because of this, the analysis and understanding of the electronic structure and magnetic properties of such materials are often incomplete.

The complexity already arises in local properties. The magnetic moment becomes nonlinear in pseudospin operators when at least four crystal-field levels are involved [6,12,13]. Even in this minimal case corresponding to pseudospin $\tilde{S} = 3/2$ (the number of crystal-field levels $N = 2\tilde{S} + 1$), each projection of magnetic moment is anisotropic and is described by as many as ten parameters. The number of parameters drastically decreases when the system has high spatial symmetry. For example, in the case of cubic symmetry (O, O_h, T_d), the $\tilde{S} = 3/2$ pseudospin state reduces to the fourfold-degenerate Γ_8 multiplet state, and the magnetic moment is expressed by only two parameters (g and G) [6]. Similarly, the number of vibronic coupling parameters decreases in the cubic environment, while the lattice dynamics becomes Jahn-Teller (JT) type [9,10,14]. The Γ_8 state appears in many systems: single-ion metal complexes [15,16], atomic clusters [17,18], and impurities in insulators and semiconductors [6,19–24]. It also arises in magnetic sites of insulators such as double perovskites containing lanthanide or heavy-transition-metal ions [25–29] and lanthanide and actinide dioxides [3,30]. In order to get deep insight into the magnetic properties of these compounds, a thorough understanding of the complex behavior of the Γ_8 multiplet is of fundamental importance.

Even in cubic systems, it is usually not easy to extract the parameters for Zeeman and vibronic interactions from experiment because of their complex interplay. On the other hand, *ab initio* methodology has proved to be a powerful tool for describing complex systems with localized electrons. With state-of-the-art quantum-chemistry methodology, it is possible to obtain nowadays accurate low-energy crystal-field states and therefore local magnetic moments and vibronic coupling constants [31]. Besides being used in the field of molecular physics and theoretical chemistry, *ab initio* quantum-chemistry methodology has been recently applied to the study of strongly correlated materials [32,33]. An important achievement was the development of *ab initio* methodology for first-principles calculations of anisotropic magnetic properties of single-ion metal centers and a unique derivation of pseudospin magnetic Hamiltonians for arbitrary multiplets [12,13,34].

In this work, we apply the *ab initio* approach to study the interplay of local vibronic and magnetic interactions in Γ_8 systems. We find that in the presence of the JT dynamics, the Zeeman interaction remains isotropic, whereas the g and G factors describing the magnetic moments change their signs with respect to the pure electronic ones. On the other hand, the static JT distortion not only makes the Zeeman interaction anisotropic in the two split Kramers doublets but also changes the sign of the g factors as a function of applied JT distortion. Finally, we calculate the Zeeman parameters for some realistic systems.

II. MODEL HAMILTONIAN FOR THE Γ_8 MULTIPLET

Consider a metal ion with an odd number of electrons in a cubic environment, allowing for the existence of Γ_8 multiplets. Hereafter, we assume that the components of Γ_8 multiplets $|\Phi_{\Gamma_8 M}\rangle$ $(M = -3/2, -1/2, 1/2, 3/2)$ transform under symmetric operations as pure spin states $|S = 3/2, M\rangle$ which are quantized along one of the C_4 axes (the z axis). According to the selection rules,

$$\left[\Gamma_8^2\right] = a_2 \oplus 2t_1 \oplus t_2, \tag{1}$$

the Γ_8 multiplet has nonzero magnetic moment (t_1 representation in cubic groups) and is able therefore to respond linearly to applied magnetic field [6]. It also couples to vibrational modes whose symmetry is defined by the antisymmetric product of

*Liviu.Chibotaru@chem.kuleuven.be

Γ_8 [9,10,14],

$$\{\Gamma_8^2\} = a_1 \oplus e \oplus t_2. \tag{2}$$

Thus, the model Hamiltonian for the Γ_8 multiplet includes the Zeeman and vibronic Hamiltonians.

The magnetic moment is usually described by using pseudospin operators since the (spin, orbital, and total) angular momenta do not commute with the Hamiltonian due to the concomitant presence of the crystal field and spin-orbit coupling [6]. The $\tilde{S}$ pseudospin states can be uniquely defined by unitary transformation of chosen N crystal-field states ($N = 2\tilde{S}+1$). The imposed constraints are that the pseudospin states transform under time-inversion and point-group symmetry operations as true angular momentum states. In the absence of sufficient symmetry and when $\tilde{S} > 1$, the pseudospin Hamiltonian can be defined via the adiabatic connection to well-established true angular momentum states [13,34]. In the general case of $\tilde{S} = 3/2$ states without point-group symmetry, the time-inversion symmetry reduces the number of the free parameters in the unitary transformation from 16 to 10 [13]. Once the pseudospin states are defined, a time-odd operator in their space is expressed by linear combination of irreducible tensor operators $Y_k^q(\tilde{\boldsymbol{S}})$ [35] of odd rank k, $k \leqslant 2\tilde{S}$, where $\tilde{\boldsymbol{S}}$ is the pseudospin operator. Accordingly, the magnetic moments μ_α ($\alpha = x,y,z$) for $\tilde{S} = 3/2$ states have terms of ranks $k = 1$ and $k = 3$, and they are expressed by 27 parameters [13,36]. The latter reduce to 2 within the cubic symmetry when the four crystal-field states correspond to the Γ_8 multiplet: one component of the magnetic moments, say, μ_z, contains only Y_1^0 and Y_3^0 operators owing to the requirement of invariance under C_4^z rotation, thus leaving only two parameters in its definition. Similarly, two parameters, g_α and G_α, will define magnetic moments for other projections α. Given the symmetry equivalence of tetragonal axes, we have $g_x = g_y = g_z = g$ and $G_x = G_y = G_z = G$. The existence of two independent parameters in the definition of $\boldsymbol{\mu}$ is also understood from the fact that Γ_8 is not simply reducible [the symmetric product $[\Gamma_8^2]$ contains two t_1 representations, Eq. (1)]; hence, t_1 operators are expressed by two reduced matrix elements. Thus, the magnetic moment for the Γ_8 state is written as [6,37]

$$\mu_\alpha = -\mu_B g O_1^\alpha(\tilde{\boldsymbol{S}}) - \mu_B G O_3^\alpha(\tilde{\boldsymbol{S}}), \tag{3}$$

where irreducible tensors O_1^α and O_3^α are defined by

$$\begin{aligned} O_1^\alpha(\tilde{\boldsymbol{S}}) &= \tilde{S}_\alpha, \\ O_3^\alpha(\tilde{\boldsymbol{S}}) &= \tilde{S}_\alpha^3 - \tfrac{1}{5}\tilde{S}_\alpha[3\tilde{S}(\tilde{S}+1) - 1]. \end{aligned} \tag{4}$$

On the other hand, the linear Jahn-Teller Hamiltonian is [9–11,38]

$$H_{\mathrm{JT}} = \sum_{\Gamma\gamma}\left[\frac{1}{2}\left(P_{\Gamma\gamma}^2 + \omega_\Gamma^2 Q_{\Gamma\gamma}^2\right)I + V_\Gamma C_{\Gamma\gamma} Q_{\Gamma\gamma}\right], \tag{5}$$

where $P_{E\gamma}$ ($\gamma = \theta,\epsilon$) and $P_{T_2\gamma}$ ($\gamma = \xi,\eta,\zeta$) are the conjugate momenta of the mass-weighted normal coordinates $Q_{E\gamma}$ and $Q_{T_2\gamma}$, respectively, ω_Γ is the frequency of the Γ mode ($\Gamma = E,T_2$), V_Γ are the linear vibronic coupling constants, I is the 4×4 unit matrix, and the matrices of the Clebsch-Gordan coefficients $C_{\Gamma\gamma}$ are defined by [39]

$$C_{E\theta} = \begin{pmatrix} 1 & 0 & 0 & 0 \\ 0 & -1 & 0 & 0 \\ 0 & 0 & -1 & 0 \\ 0 & 0 & 0 & 1 \end{pmatrix}, \quad C_{E\epsilon} = \begin{pmatrix} 0 & 0 & 1 & 0 \\ 0 & 0 & 0 & 1 \\ 1 & 0 & 0 & 0 \\ 0 & 1 & 0 & 0 \end{pmatrix},$$

$$C_{T_2\xi} = \begin{pmatrix} 0 & -i & 0 & 0 \\ i & 0 & 0 & 0 \\ 0 & 0 & 0 & i \\ 0 & 0 & -i & 0 \end{pmatrix}, \quad C_{T_2\eta} = \begin{pmatrix} 0 & -1 & 0 & 0 \\ -1 & 0 & 0 & 0 \\ 0 & 0 & 0 & 1 \\ 0 & 0 & 1 & 0 \end{pmatrix},$$

$$C_{T_2\zeta} = \begin{pmatrix} 0 & 0 & i & 0 \\ 0 & 0 & 0 & i \\ -i & 0 & 0 & 0 \\ 0 & -i & 0 & 0 \end{pmatrix}. \tag{6}$$

The components of the E representation, θ and ϵ, and the T_2 representation, ξ, η, and ζ, transform as $(2z^2 - x^2 - y^2)/\sqrt{6}$, $(x^2 - y^2)/\sqrt{2}$, $\sqrt{2}yz$, $\sqrt{2}zx$, and $\sqrt{2}xy$, respectively, under the symmetry operations. The electronic basis of the JT Hamiltonian (5) is in the increasing order of M.

III. ROLE OF THE JAHN-TELLER DYNAMICS IN THE ZEEMAN INTERACTION

We assume that the energy scale of the JT effect is larger than the Zeeman interaction. Thus, the eigenstates of the JT Hamiltonian (vibronic states) are obtained first, and then the Zeeman interaction is rewritten in the basis of the ground vibronic state.

A. Adiabatic potential-energy surface

Introducing the polar coordinates,

$$\begin{aligned} (Q_{E\theta}, Q_{E\epsilon}) &= \rho(\cos\phi, \sin\phi), \\ (Q_{T_2\xi}, Q_{T_2\eta}, Q_{T_2\zeta}) &= Q(\sin\alpha\cos\beta, \sin\alpha\sin\beta, \cos\alpha), \end{aligned} \tag{7}$$

and diagonalizing the linear vibronic term in Eq. (5), we obtain the adiabatic potential-energy surfaces (APESs; Fig. 1),

$$U_\pm(\rho, Q) = \frac{\omega_E^2}{2}\rho^2 + \frac{\omega_{T_2}^2}{2}Q^2 \pm \sqrt{V_E^2\rho^2 + V_{T_2}^2 Q^2}. \tag{8}$$

The domains for the polar coordinates are $\rho, Q \geqslant 0$, $0 \leqslant \phi < 2\pi$, $0 \leqslant \alpha \leqslant \pi$, and $0 \leqslant \beta < 2\pi$. Under the JT distortion, the

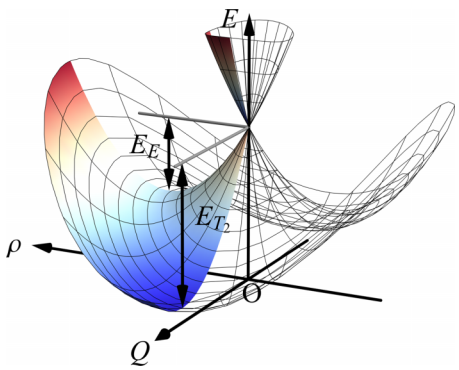

FIG. 1. The adiabatic potential-energy surface of the linear $\Gamma_8 \otimes (e \oplus t_2)$ Jahn-Teller Hamiltonian, Eq. (8). The region $\rho, Q \geqslant 0$ is colored.

Γ_8 multiplet splits into two Kramers doublets. The minima of the APES are expressed as

$$(\rho, Q, U_-) = \left(\frac{V_E}{\omega_E^2}, 0, -E_E\right), \quad \left(0, \frac{V_{T_2}}{\omega_{T_2}^2}, -E_{T_2}\right), \tag{9}$$

where E_Γ is the JT stabilization energy for the Γ vibrational mode (Fig. 1),

$$E_\Gamma = \frac{V_\Gamma^2}{2\omega_\Gamma^2} = \frac{\hbar\omega_\Gamma k_\Gamma^2}{2}, \tag{10}$$

and $k_\Gamma = V_\Gamma/\sqrt{\hbar\omega_\Gamma^3}$ is the dimensionless vibronic coupling constant.

The APES (8) and the minima (9) do not depend on the angles ϕ, α, and β, which indicates the existence of the continuum of minima along these coordinates. Thus, for $E_E > E_{T_2}$ the global minima become a one-dimensional continuum (trough) along ϕ, whereas for $E_E < E_{T_2}$ the trough is two-dimensional along α and β. Finally, when $E_E = E_{T_2}$, the energy barriers between the two minima in Eq. (9) disappear, leading to a four-dimensional trough.

B. Vibronic state

Because of the existence of the trough in the APES, the vibronic wave function is delocalized along the corresponding angular mode or coordinates. The vibronic state is a superposition of the products of the electronic and vibrational wave functions:

$$|\Psi_{\Lambda\lambda}\rangle = \sum_{M=-\tilde{S}}^{\tilde{S}} |\Phi_{\Gamma_8 M}\rangle |\chi_{\Lambda\lambda}^M\rangle. \tag{11}$$

The vibrational part $|\chi_{\Lambda\lambda}^M\rangle$ is expanded into eigenstates of the harmonic oscillators:

$$|\chi_{\Lambda\lambda}^M\rangle = \sum_{n_\theta n_\epsilon n_\xi n_\eta n_\zeta} \chi_{\Lambda\lambda}^M(\boldsymbol{n}) |n_\theta n_\epsilon n_\xi n_\eta n_\zeta\rangle, \tag{12}$$

where n_γ are the number of the vibrational quanta (indices E and T_2 are omitted for simplicity), $\boldsymbol{n} = (n_\theta, n_\epsilon, n_\xi, n_\eta, n_\zeta)$, and $\chi_{\Lambda\lambda}^M(\boldsymbol{n}) = \langle \boldsymbol{n}|\chi_{\Lambda\lambda}^M\rangle$ are decomposition coefficients. According to the general rule, the irreducible representations of the electronic state and the ground vibronic state Λ in linear JT systems coincide [10]. Thus, in the present case $\Lambda = \Gamma_8$. Using the Γ_8 ground vibronic states, $\tilde{S} = 3/2$ pseudospin can be defined following the rules discussed in the previous section.

As an example of the vibronic state (11), the expression in the weak-vibronic-coupling limit ($\hbar\omega_\Gamma \gg E_\Gamma$) within first-order perturbation is given in the Appendix. We stress that the vibronic state is not a simple product of the electronic and vibrational states as in the case of the nondegenerate system (Born-Oppenheimer approximation) but represents an entangled electron-nuclear state. In the strong-coupling case ($E_\Gamma \gg \hbar\omega_\Gamma$), the ground vibronic wave function is well described by the product of the ground adiabatic electronic state, the radial vibrational wave function (ρ, Q), and the rotational wave function in the trough (α, β, ϕ) [10,11]. For details of the linear $\Gamma_8 \otimes (e \oplus t_2)$ JT system in the strong-vibronic-coupling limit, see, e.g., Ref. [40].

In most of the existing systems, the strength of the vibronic coupling is intermediate ($E_\Gamma \approx \hbar\omega_\Gamma$). Accurate vibronic states can be obtained only by numerical diagonalization of the JT Hamiltonian matrix (5). In our numerical calculations, the vibrational basis $\{|n_\theta n_\epsilon n_\xi n_\eta n_\zeta\rangle\}$ in Eq. (12) was truncated, $0 \leqslant \sum_\gamma n_\gamma \leqslant 40$, and the Lanczos algorithm was used for the diagonalization.

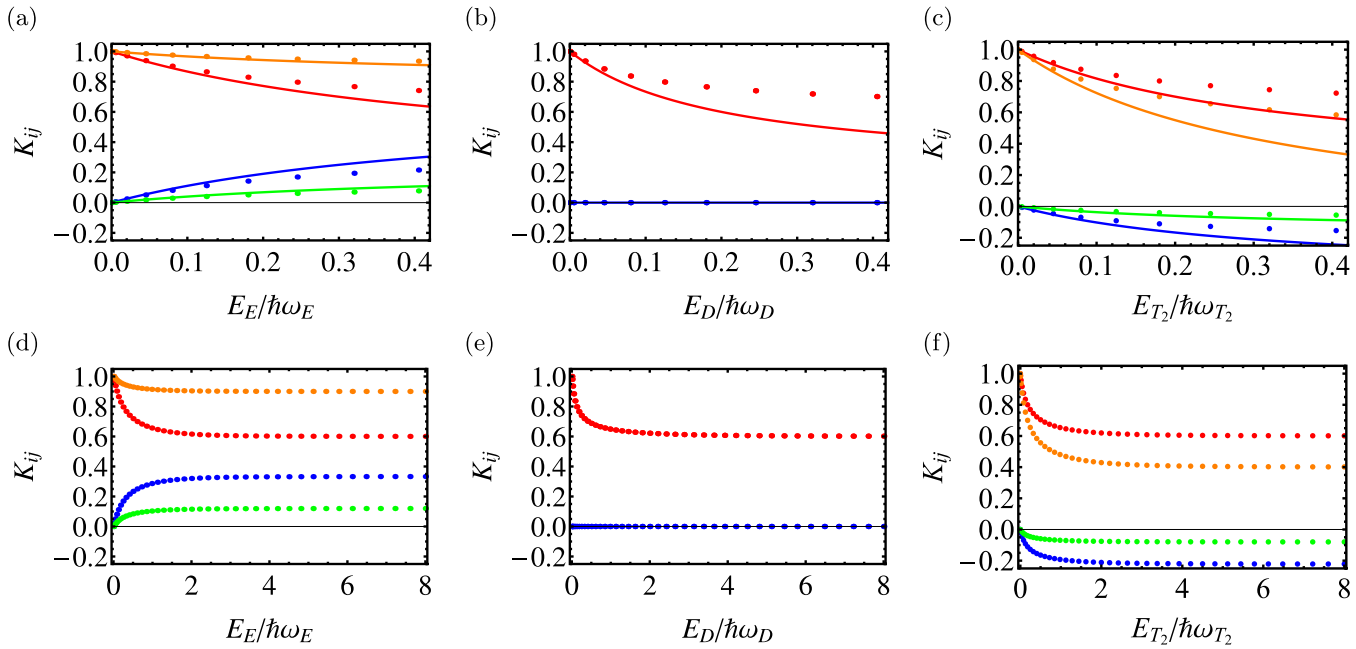

FIG. 2. Vibronic reduction factors K_{ij} as functions of the dimensionless JT stabilization energy $E_\Gamma/(\hbar\omega_\Gamma)$. The red, orange, blue, and green symbols correspond to K_{11}, K_{22}, K_{12}, and K_{21}, respectively. (a) and (d) The $\Gamma_8 \otimes e$, (b) and (e) $\Gamma_8 \otimes d$ ($k_E = k_{T_2} = k_D, \omega_E = \omega_{T_2} = \omega_D$), and (c) and (f) $\Gamma_8 \otimes t_2$ Jahn-Teller systems. The solid lines in (a), (b), and (c) correspond to the solutions in the weak-coupling limit [Eq. (14)], and the dots correspond to the numerical solutions.

C. Vibronic reduction factor

Within the space of the ground vibronic states, the electronic operators are modified by vibronic reduction factors (Ham factors) [9,10,41]. Particularly, as seen in Eq. (1), the double cubic group is not simply reducible, and each of t_1 operators is expressed by two parameters. Following Ref. [41], we introduce the vibronic reduction factors K_{ij} for $t_1(\Gamma_4)$ operators as

$$\begin{aligned}\langle\Psi_{\Gamma_8 M}|O_1^z(\tilde{\boldsymbol{S}})|\Psi_{\Gamma_8 M}\rangle &= K_{11}O_1^z(M) + K_{12}O_3^z(M),\\ \langle\Psi_{\Gamma_8 M}|O_3^z(\tilde{\boldsymbol{S}})|\Psi_{\Gamma_8 M}\rangle &= K_{21}O_1^z(M) + K_{22}O_3^z(M),\end{aligned} \quad (13)$$

where $O_k^z(M) = \langle\Phi_{\Gamma_8 M}|O_k^z(\tilde{\boldsymbol{S}})|\Phi_{\Gamma_8 M}\rangle$.

In the weak-vibronic-coupling limit (see the Appendix), the reduction factors are calculated as

$$\begin{aligned}K_{11} &= \frac{5 + k_E^2 + 3k_{T_2}^2/2}{5\left(1 + k_E^2 + 3k_{T_2}^2/2\right)},\\ K_{12} &= \frac{2\left(k_E^2 - k_{T_2}^2\right)}{3\left(1 + k_E^2 + 3k_{T_2}^2/2\right)},\\ K_{21} &= \frac{9}{25}K_{12},\\ K_{22} &= \frac{5 + 4k_E^2 - 3k_{T_2}^2/2}{5\left(1 + k_E^2 + 3k_{T_2}^2/2\right)}.\end{aligned} \quad (14)$$

The reduction factors significantly depend on the type of the Jahn-Teller effect. When $|k_E| > |k_{T_2}|$, we obtain $K_{11} < K_{22}$ and $K_{12}, K_{21} > 0$, while when $|k_E| < |k_{T_2}|$, $K_{11} > K_{22}$ and $K_{12}, K_{21} < 0$. These relations for K_{12} and K_{21} hold for any strength of the vibronic coupling [41]. The solid lines in Figs. 2(a)–2(c) are calculated reduction factors in Eq. (14) with respect to the vibronic coupling strength for various situations.

Figure 2(e) shows good agreement with the simulation in Ref. [42]. In comparison to numerical results, the reduction factors within the perturbation theory are quantitatively correct only for $E_\Gamma/\hbar\omega_\Gamma \lesssim 0.1$, while their qualitative properties such as the sign and the order of K_{ij} are well described even for larger E_Γ [Figs. 2(a)–2(c)]. Figures 2(d)–2(f) show that the reduction factors are saturated around $E_\Gamma/\hbar\omega_\Gamma \approx 1$.

D. g factors

In the ground vibronic states, the magnetic moment operators are calculated as follows:

$$\mu'_\alpha = -\mu_B g' O_1^\alpha(\tilde{\boldsymbol{S}}) - \mu_B G' O_3^\alpha(\tilde{\boldsymbol{S}}), \quad (15)$$

where g' and G' are defined by

$$g' = K_{11}g + K_{21}G, \quad G' = K_{12}g + K_{22}G, \quad (16)$$

respectively, using Eq. (13). The pseudospin operator $\tilde{\boldsymbol{S}}$ in Eq. (15) acts on the ground Γ_8 vibronic states. As Eq. (15) shows, the Zeeman pseudospin Hamiltonian remains isotropic as in Eq. (3).

Figures 3(a)–3(c) show g'/g and G'/g as a function of G/g for the $\Gamma_8 \otimes e$, $\Gamma_8 \otimes d$, and $\Gamma_8 \otimes t_2$ models, respectively. Because of the reduction factors K_{ij}, g' and G' can change their signs [23]. In particular, for the $\Gamma_8 \otimes e$ and $\Gamma_8 \otimes t_2$ JT systems, there are regions of G/g where the sign of G'/g becomes opposite that of G/g. Figures 3(d)–3(f) show the Zeeman splitting as a function of g/G. The difference between the Zeeman splittings by electronic g, G (dashed lines) and those by vibronic g', G' (solid lines) is evidently significant. The Zeeman splittings are significantly modified by the JT

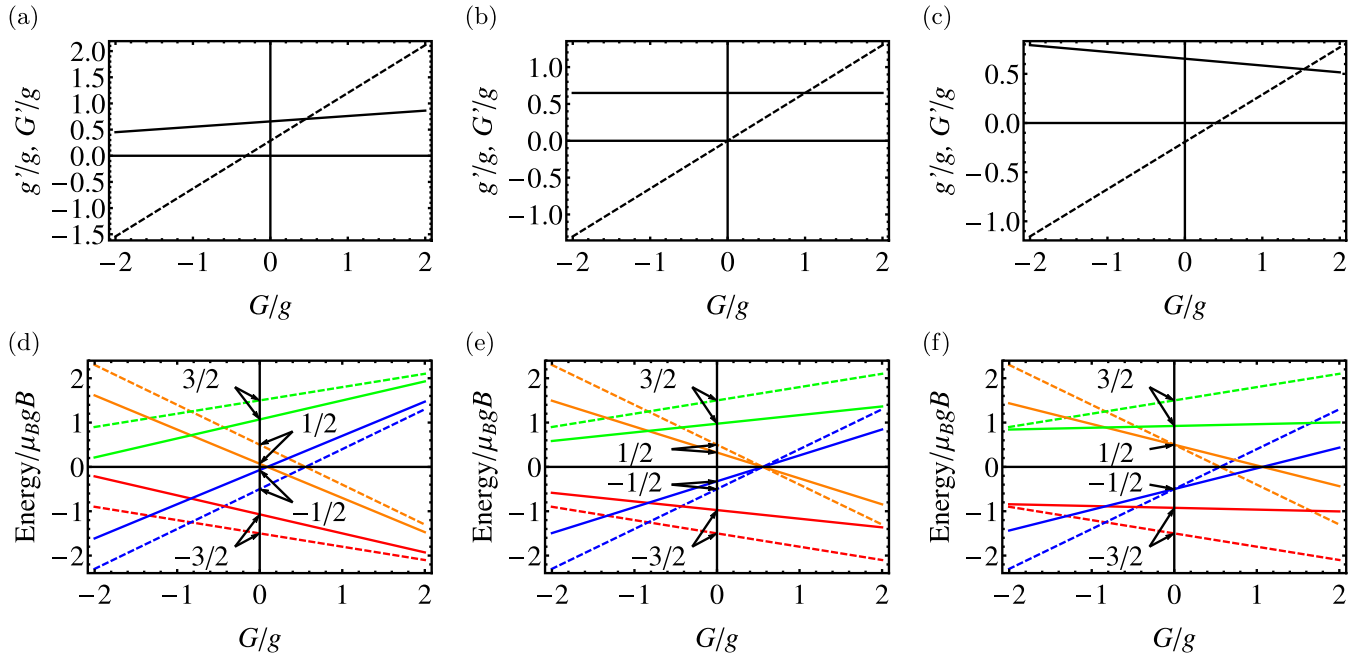

FIG. 3. g' and G' for (a) $\Gamma_8 \otimes e$, (b) $\Gamma_8 \otimes d$, and (c) $\Gamma_8 \otimes t_2$ JT systems. The ratios g'/g (solid lines) and G'/g (dashed lines) are given as a function of G/g. The energy levels of (d) $\Gamma_8 \otimes e$, (e) $\Gamma_8 \otimes d$, and (f) $\Gamma_8 \otimes t_2$ JT systems as a function of G/g without (dashed lines) and with (solid lines) the dynamical JT effect. The numbers $-3/2, -1/2, 1/2$, and $3/2$ are the momentum projection of the vibronic states. For the calculations, the data with $k_\Gamma = 1.4$, when the reduction factors are saturated, were used.

dynamics, and the crossing point (G/g) of the Zeeman levels is also shifted due to the JT effect. Thus, the interpretation of EPR and related experiments based solely on the electronic multiplets could be incorrect.

IV. ROLE OF THE STATIC JAHN-TELLER DISTORTION IN THE ZEEMAN INTERACTION

When the higher-order vibronic couplings are also important and the trough is strongly warped to mix several low-energy vibronic states, the ground vibronic state is localized at minima; that is, the static JT effect arises. Let us consider the case where the splitting of the Γ_8 states is large compared with the Zeeman splitting of each Kramers doublets. In such cases, it is convenient to introduce the pseudospin $\tilde{S} = 1/2$ for each Kramers doublet following the methodology described in Refs. [12,13].

The magnetic moment within the lower adiabatic electronic states is $\boldsymbol{\mu}'' = \sum_{r,r'=1}^{2} \langle \Phi_r | \boldsymbol{\mu} | \Phi_{r'} \rangle | \Phi_r \rangle \langle \Phi_{r'} |$, where $|\Phi_r(\Omega)\rangle$ ($r = 1,2$) are the components of the ground Kramers doublet and $\Omega = (\phi,\alpha,\beta)$ is the set of angles in Eq. (7). Since $|\Phi_r\rangle$ depends on the JT distortion Ω, $\boldsymbol{\mu}''$ and g_i are also functions of Ω.

Figures 4(a)–4(c) show g_i ($i = X,Y,Z$) as a function of ϕ at various G/g for the case $E_E > E_{T_2}$. Due to the JT distortion, the g tensor becomes anisotropic, whereas the main magnetic axes in the distorted geometries are directed along the tetragonal axes [Fig. 4(f)] since the JT distortion along e modes preserve them as symmetry axes. Even for fixed G/g, e.g., $G/g = 3/4$ [Fig. 4(a)], the JT distortion can change the nature of the magnetic moment from easy plane ($g_X = g_Y > g_Z$ at $\phi = 0$) to axial ($g_Y > g_X = g_Z$ at $\phi = \pi/3$).

It is interesting to see the evolution of the sign of product $g_X g_Y g_Z$, defining the direction of the Larmor precession of the magnetic moment, the pattern of the hyperfine splitting (nuclear quadrupole moment) [43], and the sign of the Berry phase [44]. The sign of $g_X g_Y g_Z$ can be found by calculating $g_i g_j / g_k$ from the expression [43]

$$\left[\mu_i'', \mu_j''\right] = -i\mu_B \frac{g_i g_j}{g_k} \mu_k'', \tag{17}$$

where (i,j,k) is a cyclic permutation of (X,Y,Z). $g_i g_j / g_k$ is shown in Figs. 4(d) and 4(e) as a function of the angle ϕ. The calculation shows that the sign changes for some G/g. The change in sign occurs at a value of ϕ when one of the g factors become zero at a point [Figs. 4(b) and 4(c)]. Thus, the sign of the product of the g factors is sensitive to the local JT distortion as well as the nature of the Γ_8 electronic states via the ratio G/g.

Figures 5(a)–5(c) show g_i ($i = X,Y,Z$) as functions of the t_2 JT distortions and angular coordinates α and β for the case $E_{T_2} > E_E$. Contrary to the $\Gamma_8 \otimes e$ JT system, the sign of the product $g_X g_Y g_Z$ does not change with respect to the JT distortion [Fig. 5(d)]. In the case of the $\Gamma_8 \otimes t_2$ JT system, however, both the values of g_i and the directions of the main magnetic axes vary with distortions [Figs. 5(e) and 5(f) for $G/g = 1$ and -1, respectively]. The nature of the main magnetic axes g_i depends on the value of G/g. Thus, for $G/g = 1$ the anisotropy is of easy-axis type [Figs. 5(a) and 5(e)], whereas it is of easy-plane type for $G/g = -1$ [Figs. 5(c) and 5(f)].

V. *AB INITIO* DERIVATION OF THE Γ_8 HAMILTONIAN

As examples illustrating the obtained results, g and G factors and vibronic couplings of the Cs_2ZrCl_6:Np^{4+} impurity

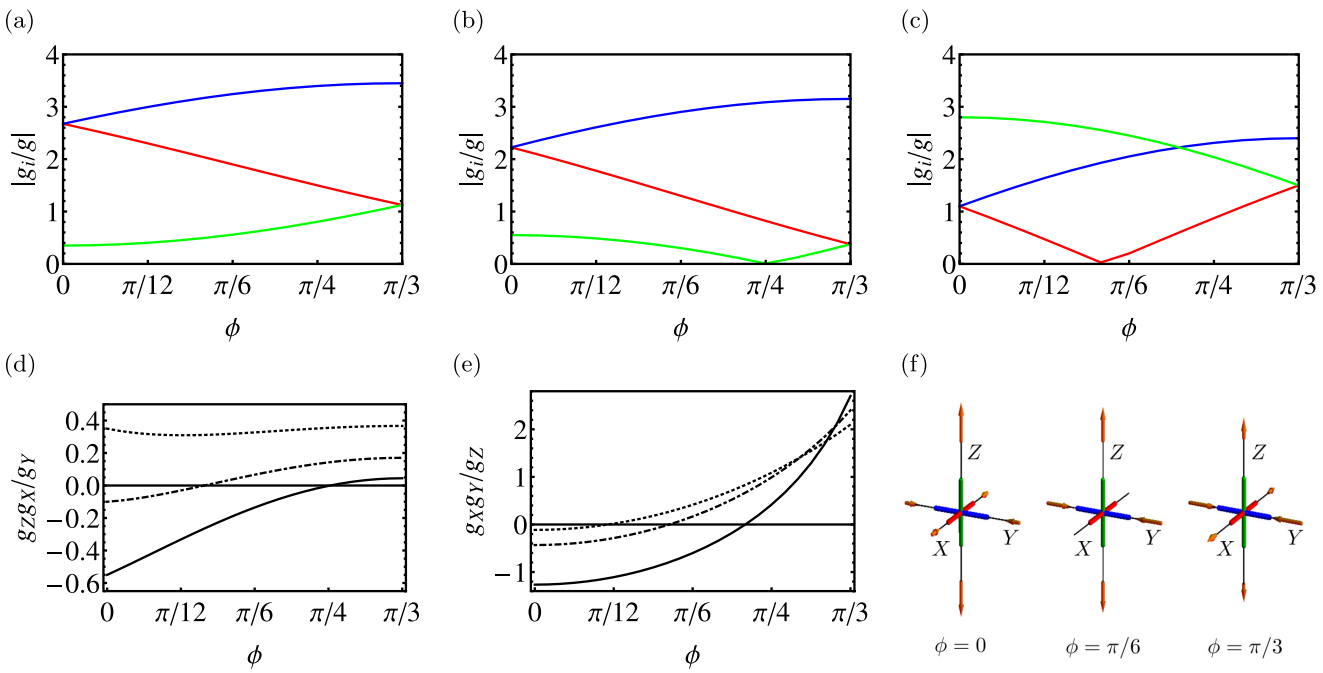

FIG. 4. (a)–(c) g_i ($i = X,Y,Z$), (d) and (e) the signs of $g_X g_Y g_Z$, and (f) the main magnetic axes as functions of the angle ϕ of the static e JT distortion. g_i are calculated in the unit of g. For the calculations of the g factors, (a) $G/g = 3/4$, (b) $1/4$, and (c) -1 are used. (d) $g_Z g_X / g_Y$ for $G/g = 1/4, 1/2, 3/4$ (solid, dot-dashed, and dotted curves, respectively), and (e) $g_X g_Y / g_Z$ for $G/g = -1/2, -1, -3/2$ (solid, dot-dashed, and dotted curves, respectively). The orange arrows in (f) indicate the JT displacements of atoms.

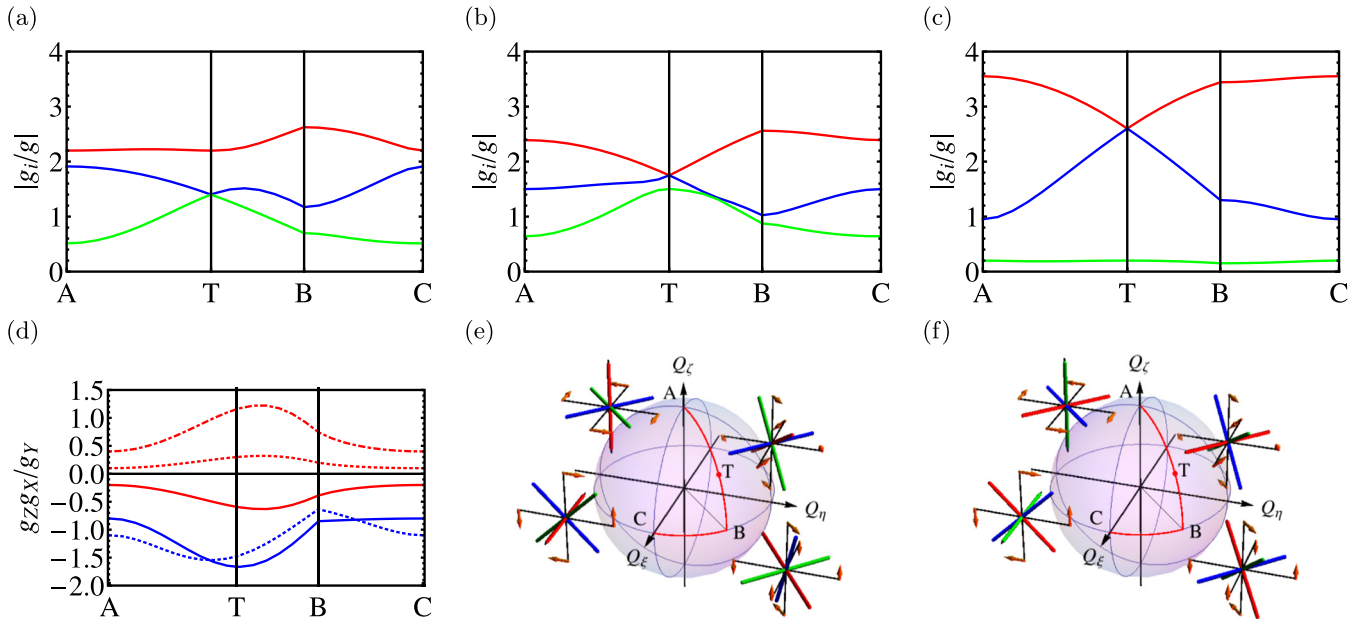

FIG. 5. (a)–(c) g_i ($i = X,Y,Z$), (d) the product of the g factors, and (e) and (f) the magnetic axes as functions of the Euler angles of the static t_2 JT distortion. g_i are calculated in units of g. For the calculations of the g factors, (a) $G/g = 1$, (b) $5/12$, and (c) -1 were used. (d) $g_Z g_X/g_Y$ for $G/g = -3/2,-1,-1/2,1/2,1$ (red dot-dashed, red dotted, red solid, blue solid, and blue dotted curves, respectively) are shown. The magnetic axes are obtained for (e) $G/g = 1$ and (f) -1. The T (trigonal) point corresponds to $Q_\xi = Q_\eta = Q_\zeta$.

in an octahedral zirconium site [20–22] and of the ThO_2:Ir^{4+} impurity in a cubic thorium site are further calculated.

A. Computational methodology

The low-lying electronic states of the impurity are obtained from cluster calculations. The electronic structures are calculated combining the complete-active-space self-consistent-field (CASSCF), extended multi-state complete active space second-order perturbation theory (XMS-CASPT2) [45,46] (for Ir^{4+}), and spin-orbit restricted-active-space state-interaction (SO-RASSI) methods implemented in the MOLCAS package [47]. The cluster consists of one impurity ion surrounded by several layers of ions. The impurity and the closest atoms are treated *ab initio*, whereas the others are replaced by embedding *ab initio* model potentials (AIMPs).

In the former system, the Np^{4+} ion and the closest six chlorine and eight cesium ions are treated *ab initio* (Fig. 6). Atomic-natural-orbital relativistic-correlation consistent-minimal basis (ANO-RCC-MB) (MB), atomic-natural-orbital relativistic-correlation consistent-valence double zeta polarization (ANO-RCC-VDZP) (DZP), and atomic-natural-orbital relativistic-correlation consistent-valence triple zeta polarization (ANO-RCC-VTZP) (TZP) basis sets were used for the Np^{4+} and closest chlorine ions and effective core potential (ECP)-AIMP was used for the closest eight cesium ions [48], which included the last seven electrons in the basis. Contraction of the employed basis sets is given in the Supplemental Material [49]. The next two layers of atoms are described by AIMPs with no electrons (frozen density). Optimization of these potentials was done within the iterative self-consistent embedding-ion (SCEI) methodology [50] employed earlier. For these calculations we used similarly sized basis sets for individual atoms. In this approach, *ab initio* self-consistent calculations are carried out for each atom in the field of model potentials of other atoms. The SCEI procedure is carried out until full self-consistency between potentials of all atoms is achieved ($\Delta E < 10^{-7}$ a.u.). Optimized AIMPs for the individual atoms in Cs_2ZrCl_6 are given in [49]. The active space consisted of three electrons in seven $4f$-type orbitals. All spin-free states (35 quartet and 112 doublet states) were mixed by spin-orbit coupling within the RASSI program.

In the latter system, the Ir^{4+} ion and the closest eight oxygen atoms were treated *ab initio* by employing the ANO-RCC-VDZP basis set. In order to simulate the effect of the envi-

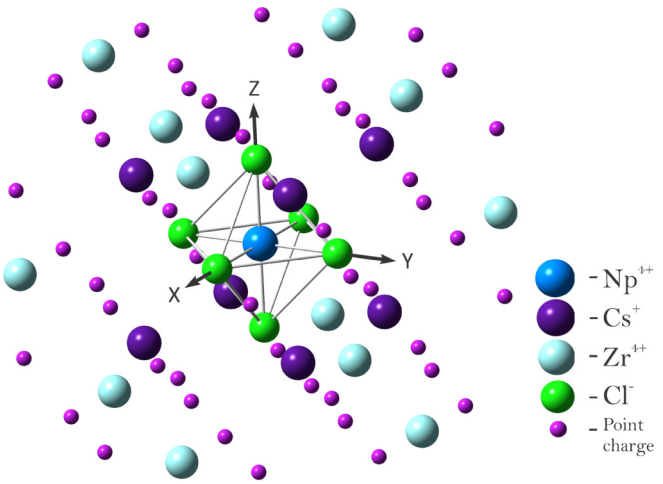

FIG. 6. The calculated Cs_2ZrCl_6:Np^{4+} cluster (see the text for details).

ronment, distant thorium and oxygen atoms were described computationally by AIMP [51,52]. The active space of the CASSCF method comprised 11 electrons in eight orbitals (five $5d$-type orbitals of Ir^{4+} and three t_{2g}-type orbitals of the ligand). Seventy-five doublet states ($S = 1/2$) were optimized variationally. In the multistate XMS-CASPT2 calculation only the lowest three roots were considered, which were later mixed by spin-orbit coupling at the SO-RASSI stage.

B. Definition of pseudospin from *ab initio* calculations

The proper transformation of *ab initio* Γ_8 crystal-field states into Γ_8 pseudospin states is a crucial step for the unique definition of the pseudospin states. The crystal-field states are generally arbitrary linear combinations of the pseudospin states. However, in the present case, due to high symmetry of the complexes, the eigenstates of the magnetic moment projections along the main magnetic axes (tetragonal axes) correspond already to definite components of Γ_8 pseudospin states $|\Phi_{\Gamma_8 M}\rangle$. This is also seen in the structure of the component of the magnetic moments, Eqs. (3) and (4), which contains only powers of the corresponding pseudospin projection. We further denote the eigenstates of μ_z as a, b, c, d in increasing order of their eigenvalues. These eigenstates fulfill the time-reversal symmetry: under time inversion, a and b transform into d and c, respectively. However, there still remain eight possible assignments of the eigenstates to $|\Phi_{\Gamma_8 M}\rangle$; $(a,b,c,d) = (\mp 3/2, \mp 1/2, \pm 1/2, \pm 3/2), (\mp 3/2, \pm 1/2, \mp 1/2, \pm 3/2), (\mp 1/2, \mp 3/2, \pm 3/2, \pm 1/2)$, and $(\mp 1/2, \pm 3/2, \mp 3/2, \pm 1/2)$. This issue is completely solved by analyzing the rotational symmetry properties of states a–d.

For the assignment of multiconfigurational states a–d, it is sufficient to find symmetrized electron configurations which transform properly under symmetry operations. This is done straightforwardly by identifying the contributions of the true S configurations in the eigenstates. For example, in the case of the f^3 system (Np^{4+}), the spin states $|SM\rangle$ of the admixed electronic term $^4A_2$ originating from the $6p^3$ configuration of actinide can easily be put in relation to $|\Gamma_8, M\rangle$, which coincides with that of Γ_8 pseudospin states. Details of this assignment for Np^{4+} and Ir^{4+} are shown below.

TABLE I. *Ab initio* (MB, DZP, TZP) and experimental (Expt.) g, G and g', G' for the Np^{4+} ion. MB, DZP, and TZP indicate the basis set.

	Ab initio			Expt.
	MB	DZP	TZP	
g	0.334	0.364	0.366	
G	−1.860	−1.918	−1.925	
g'	0.335	0.364	0.366	0.36
G'	−1.823	−1.880	−1.887	−2.25

C. Weak vibronic coupling: Cs_2ZrCl_6:Np^{4+}

The low-energy states of Np^{4+} are described by the crystal-field split $J = 9/2$ atomic multiplet, and it has been found that the ground state of the Np^{4+} impurity is the Γ_8 state. Our *ab initio* calculations reproduce the Γ_8 ground state. The assignment of the Γ_8 state is done by comparing the $^4A_2$ configurations admixed to the Γ_8 states and the relation between the Γ_8 representation and the product of the A_2 and Γ_8 ($S = 3/2$) representations [39]:

$$|\Gamma_8, \mp 3/2\rangle = |^4A_2, \pm 1/2\rangle, \quad |\Gamma_8, \mp 1/2\rangle = -|^4A_2, \pm 3/2\rangle,$$

where $|^4A_2, M\rangle$ is spin-orbital decoupled state and M is the z projection of the spin. The g and G parameters calculated with three basis sets are shown in Table I. The results with the double-zeta and triple-zeta basis sets are close to each other. Thus, hereafter, we use the double-zeta basis set for the calculations of Np^{4+}.

The vibronic coupling constants k_Γ and the frequencies of $NpCl_6^{2-}$ are derived by fitting the model APES, Eq. (8), to the APES obtained in *ab initio* calculations. Since the octahedral system has only one e_g vibrational mode and one t_{2g} vibrational mode, the corresponding displacements are determined by symmetry [Figs. 7(a) and 7(b)] [10,11]. The APESs with respect to the $e_g\theta$ and $t_{2g}\zeta$ JT distortions are shown in Figs. 7(c) and 7(d), respectively [53]. The red points are the *ab initio* APESs with respect to the JT distortion, and the black solid lines are the simulations with Eq. (8). The best-fitted frequencies and the dimensionless vibronic coupling constants are $\omega_E = 618$ cm^{-1}, $\omega_T = 157$ cm^{-1}, $k_E = 0.035$, and $k_T = 0.111$. Although the existence of the

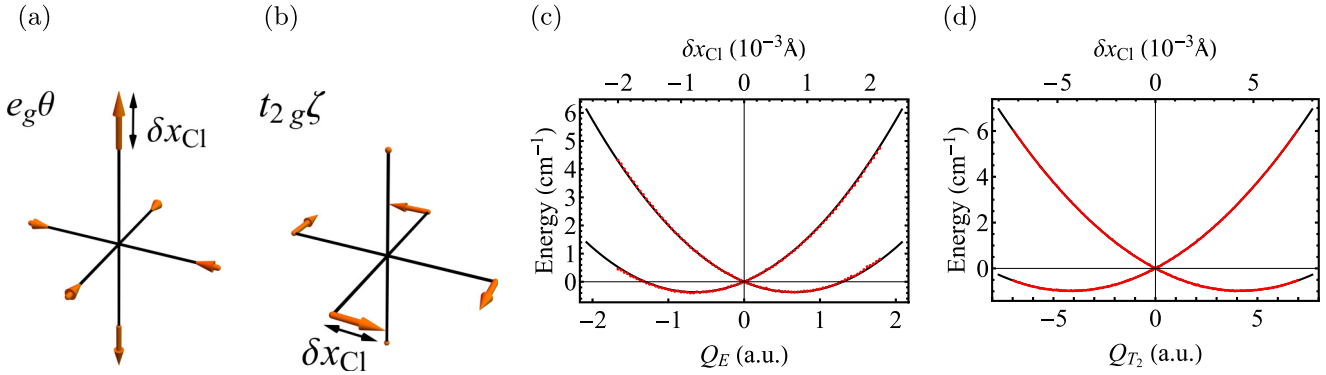

FIG. 7. (a) and (b) The $e_g\theta$ and $t_{2g}\xi$ vibrational modes. The Γ_8 APESs of the $[NpCl_6]^{2-}$ complex with respect to (c) $e_g\theta$ and (d) $t_{2g}\xi$ JT distortions (meV). The red points are the *ab initio* results, and the black solid lines are the APESs fitted with Eq. (8). The JT distortions are measured by the displacement of the Cl atom δx_{Cl} (10^{-3} Å), as shown in (a) and (b).

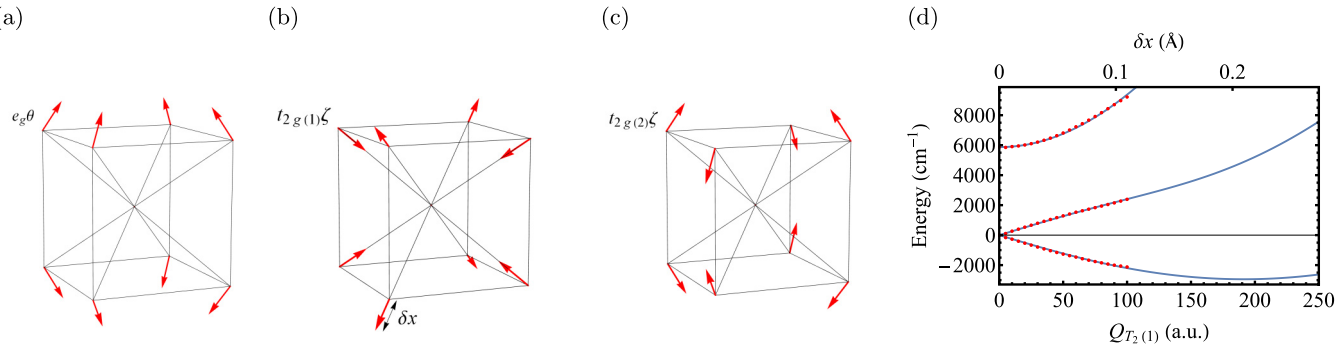

FIG. 8. (a)–(c) The $e_g\theta$, $t_{2g}(1)\zeta$, and $t_{2g}(2)\zeta$ distortions of a cube. (d) The APESs with respect to $t_{2g(1)}\zeta$ JT distortion. The red points correspond to the *ab initio* calculations, while the black lines are the fitted APESs. δx shows the displacement of O atoms in (b).

JT effect in this complex has been anticipated [20,54], its role is now found to be negligible. One of the reasons why the vibronic coupling is so weak is explained by the fact that the ground molecular term in the absence of spin-orbit coupling is the orbitally nondegenerate $^4A_2$ according to CASSCF calculations. The second reason is the relatively localized nature of the $5f$ orbitals.

With the use of the vibronic coupling constants and vibrational frequencies, we calculated the vibronic states by numerical diagonalization of the JT Hamiltonian (see Sec. III B). The vibronic reduction factors are $K_{11} = 0.985$, $K_{12} = -0.007$, $K_{21} = -0.003$, and $K_{22} = 0.979$. The obtained g' and G' (16) are given in Table I. The calculated g' and G' are close to g and G, respectively, as a result of weak vibronic coupling in the Γ_8 multiplet. They are in good agreement with the experimental values listed in Table I [55]. The obtained discrepancy for G (G') may be attributed to insufficient accuracy of *ab initio* calculations, which did not include the CASPT2 step.

A similar situation takes place in $[(CH_3)_4N]_2NpCl_6$ [56] and in NpO_2. Although in the latter system the JT effect is stronger than in $NpCl_6^{2-}$ due to the presence of more covalent oxygen ligands, the ratio between E_{JT} and the vibrational quantum corresponding to the JT-active distortions will still be very small as in isostructural UO_2 [57]. For this reason, according to Eqs. (14), the manifestation of the JT effect on the magnetic moments is expected to be unimportant.

D. Strong vibronic coupling: ThO_2:Ir^{4+}

Stronger vibronic coupling is expected when the overlap of the magnetic orbitals and the ligand orbitals is large. This seems to be the case for $5d$ ions such as Ir^{4+}. In a cubic environment, the atomic d shell splits into e_g and t_{2g} levels, the latter being higher in energy. Hence, in the case of the $5d^5$ configuration of Ir^{4+} the e_g levels are fully occupied, and the t_{2g} levels are singly occupied. The CASSCF/CASPT2 calculations confirm this picture, showing that the ground state of the Ir^{4+} center corresponds to $S = 1/2$ (without spin-orbit coupling), mainly coming from the configuration $e_g^4 t_{2g}^1$. In the presence of spin-orbit coupling, the $^2T_{2g}$ term splits into ground Γ_8 and excited Γ_7 states. The ground Γ_8 multiplet states are assigned by analyzing the contributions of $^2T_{2g}$ in comparison with the symmetry relation between the direct product $T_{2g} \otimes \Gamma_6$ ($S = 1/2$) and the Γ_8 representation [39]:

$$|\Gamma_8, \mp 3/2\rangle = \mp\frac{i}{\sqrt{6}}|^2T_{2g}\xi, \mp 1/2\rangle + \frac{1}{\sqrt{6}}|^2T_{2g}\eta, \mp 1/2\rangle + i\sqrt{\frac{2}{3}}|^2T_{2g}\zeta, \pm 1/2\rangle,$$

$$|\Gamma_8, \mp 1/2\rangle = \pm\frac{i}{\sqrt{2}}|^2T_{2g}\xi, \pm 1/2\rangle - \frac{1}{\sqrt{2}}|^2T_{2g}\eta, \pm 1/2\rangle,$$

where $|^2T_{2g}\gamma, M\rangle$ is the term's wave function and γ ($= \xi, \eta, \zeta$) and M ($= \pm 1/2$) are the orbital and spin components, respectively. The g and G parameters are obtained as -0.076 and 0.169, respectively. The small g and G are explained by the partial cancellation of the orbital and spin angular momenta [58].

The cubic system contains one e_g [Fig. 8(a)] and two t_{2g} [Figs. 8(b) and 8(c)] vibrational modes. The APES with respect to the $t_{2g}(1)$ distortion shows a very large JT stabilization energy [Fig. 8(d)], whereas those for e_g and $t_{2g}(2)$ are negligibly small (APESs are not shown). The red points in Fig. 8(d) correspond to the *ab initio* APES, which shows huge Jahn-Teller splitting. The strong vibronic coupling to the $t_{2g}(1)$ mode is due to both the delocalization of the $5d$ orbitals and the distortion along the Ir-O bond [see Fig. 8(b)], while the couplings to the e_g and $t_{2g}(2)$ modes are small because the displacements are perpendicular to the Ir-O bonds [Figs. 8(a) and 8(c)]. Figure 8(d) also shows that the upper level of the Γ_8 state does not follow a parabola as expected from Eq. (8). The discrepancy is expected to originate from the vibronic coupling between the ground Γ_8 states and the excited Γ_7 states. Accordingly, we include in our analysis of the APESs the excited Kramers doublet. The JT Hamiltonian in this case consists of the Γ_8 part given in Eq. (5), the vibrational Hamiltonian ($\Delta E + \sum_{\Gamma\gamma} \frac{1}{2}\omega'_\Gamma{}^2 Q'^2_\gamma$) for the Γ_7 multiplets (ΔE is the excitation energy of the Γ_7 level with respect to the ground Γ_8 level, and ω'_Γ is the frequency), and the cross vibronic terms between the Γ_8 and Γ_7 multiplets:

$$U' = \sum_{\Gamma\gamma}(V'_\Gamma C'_{\Gamma\gamma} Q_{\Gamma\gamma} + \text{H.c.}), \tag{18}$$

where V'_Γ are real off-diagonal vibronic coupling constants and $C'_{\Gamma\gamma}$ are defined by

$$C'_{E\theta}=\begin{pmatrix}0&-1\\0&0\\0&0\\1&0\end{pmatrix},\quad C'_{E\epsilon}=\begin{pmatrix}0&0\\1&0\\0&-1\\0&0\end{pmatrix},$$
$$C'_{T_2\xi}=\begin{pmatrix}i\frac{\sqrt{3}}{2}&0\\0&\frac{i}{2}\\-\frac{i}{2}&0\\0&-i\frac{\sqrt{3}}{2}\end{pmatrix},\quad C'_{T_2\eta}=\begin{pmatrix}\frac{\sqrt{3}}{2}&0\\0&\frac{1}{2}\\\frac{1}{2}&0\\0&\frac{\sqrt{3}}{2}\end{pmatrix},$$
$$C'_{T_2\zeta}=\begin{pmatrix}0&0\\i&0\\0&i\\0&0\end{pmatrix}. \tag{19}$$

The bases for the rows and the columns of $C'_{\Gamma\gamma}$ are the Γ_8 and Γ_7 states in increasing order of M. Applying the second-order perturbation theory, the APESs are expressed as

$$\begin{aligned}U^{\Gamma_8}_{\pm}(Q)&=\tfrac{1}{2}\omega^2_{T_2}Q^2_{T_{2g}\zeta}\pm V_{T_2}Q_{T_{2g}\zeta}\\&\quad+\frac{\frac{1}{2}V'^2_{T_2}Q^2_{T_2\zeta}}{-\Delta E+\frac{1}{2}\left(\omega^2_{T_2}-\omega'^2_{T_2}\right)Q^2_{T_2\zeta}\pm V_{T_2}Q_{T_2\zeta}},\\U^{\Gamma_7}(Q)&=\Delta E+\tfrac{1}{2}\omega'^2_{T_2}Q^2_{T_2\zeta}\\&\quad+\sum_{\sigma=\pm}\frac{\frac{1}{2}V'^2_{T_2\zeta}Q^2_{T_2\zeta}}{\Delta E-\frac{1}{2}\left(\omega^2_{T_2}-\omega'^2_{T_2}\right)Q^2_{T_2\zeta}+\sigma V_{T_2}Q_{T_2\zeta}}.\end{aligned} \tag{20}$$

The best fitting of the *ab initio* APESs to Eq. (20) is given by $V_{T_2}=1.17\times10^{-4}$ a.u., $\omega_{T_2}=191.32\,\mathrm{cm}^{-1}$, $V'_{T_2}=1.37\times10^{-4}$ a.u., and $\omega'_{T_2}=298.63\ \mathrm{cm}^{-1}$ [solid lines in Fig. 8(d)]. The calculated dimensionless vibronic coupling constant $k_{T_2}=4.54$ indicates that Ir^{4+} will show a strong JT effect ($E_{T_2(1)}$ exceeds $\hbar\omega_{T_2(1)}$ by several times).

With the obtained vibronic coupling constants, we calculated the reduction factors as follows: $K_{11}=0.60$, $K_{12}=-0.079$, $K_{21}=-0.22$, and $K_{22}=0.40$. For simplicity, the Γ_7 states were not taken into account in the simulation. Using the reduction factors K_{ij}, we obtain $g'=-0.083$ and $G'=0.074$. As expected for a large vibronic coupling, G' differs greatly from G ($g=-0.076$ and $G=0.169$).

VI. CONCLUSIONS

In this work, we investigated thoroughly the interplay between the Zeeman interaction and the Jahn-Teller effect in the Γ_8 multiplet. Combining the theory and *ab initio* quantum-chemistry calculations, we demonstrated the role of the Jahn-Teller effect on the magnetic moment. This was achieved by using an *ab initio* methodology of the derivation of the Zeeman pseudospin Hamiltonian and of the vibronic parameters of the $\Gamma_8\otimes(e\oplus t_2)$ JT Hamiltonian. The main conclusions are the following:

(1) The dynamical JT effect can modify not only the absolute values of the parameters of the Zeeman pseudospin Hamiltonian but also their signs with respect to pure electronic case.

(2) In the presence of the static JT distortion, the nature of the magnetic moments depends on the type of distortion as well as on the values of the g factors. In particular, the sign of $g_X g_Y g_Z$ can change due to the rotation of the JT distortion, which could be experimentally observed using a circular polarized magnetic field or in hyperfine spectra.

The strong Jahn-Teller coupling of Ir^{4+} impurity in a cubic site predicted by our *ab initio* calculations is intriguing because of the lack of the experimental study of the strong Jahn-Teller effect in Γ_8 systems. The present *ab initio* approach allowing for quantitative study of the interplay of the Zeeman and vibronic interactions will be useful for the study of various Γ_8 and other multiplet states in complexes and correlated materials. Further applications of the present methodology will be discussed elsewhere.

ACKNOWLEDGMENTS

N.I. is supported by a Japan Society for the Promotion of Science (JSPS) Overseas Research Fellowship. He would like also to acknowledge the financial support from the Fonds Wetenschappelijk Onderzoek-Vlaanderen (FWO) and the GOA Grant from KU Leuven. V.V. and L.U. are supported by postdoctoral fellowships from FWO.

APPENDIX: VIBRONIC STATE IN THE WEAK VIBRONIC COUPLING

Within the first order of perturbation theory, the ground vibronic states are given as

$$\begin{aligned}|\Psi_{\Gamma_8\frac{3}{2}}\rangle&=N\Big[|\Phi_{\Gamma_8\frac{3}{2}}\rangle|00000\rangle-\frac{k_E}{\sqrt{2}}|\Phi_{\Gamma_8\frac{3}{2}}\rangle|10000\rangle\\&\quad-\frac{k_E}{\sqrt{2}}|\Phi_{\Gamma_8-\frac{1}{2}}\rangle|01000\rangle+\frac{ik_{T_2}}{\sqrt{2}}|\Phi_{\Gamma_8\frac{1}{2}}\rangle|00100\rangle\\&\quad+\frac{k_{T_2}}{\sqrt{2}}|\Phi_{\Gamma_8\frac{1}{2}}\rangle|00010\rangle+\frac{ik_{T_2}}{\sqrt{2}}|\Phi_{\Gamma_8-\frac{1}{2}}\rangle|00001\rangle\Big],\\|\Psi_{\Gamma_8\frac{1}{2}}\rangle&=N\Big[|\Phi_{\Gamma_8\frac{1}{2}}\rangle|00000\rangle+\frac{k_E}{\sqrt{2}}|\Phi_{\Gamma_8\frac{1}{2}}\rangle|10000\rangle\\&\quad-\frac{k_E}{\sqrt{2}}|\Phi_{\Gamma_8-\frac{3}{2}}\rangle|01000\rangle+\frac{ik_{T_2}}{\sqrt{2}}|\Phi_{\Gamma_8\frac{3}{2}}\rangle|00100\rangle\\&\quad-\frac{k_{T_2}}{\sqrt{2}}|\Phi_{\Gamma_8\frac{3}{2}}\rangle|00010\rangle-\frac{ik_{T_2}}{\sqrt{2}}|\Phi_{\Gamma_8-\frac{3}{2}}\rangle|00001\rangle\Big],\end{aligned} \tag{A1}$$

where N is the normalization constant, $N=1/\sqrt{1+k_E^2+3k_{T_2}^2/2}$. Substituting Eq. (A1) into Eq. (13) and solving that system of equations, we obtain Eq. (14).

[1] R. Sessoli and A. K. Powell, Strategies towards single molecule magnets based on lanthanide ions, Coord. Chem. Rev. **253**, 2328 (2009).

[2] *Lanthanides and Actinides in Molecular Magnetism*, edited by R. Layfield and M. Murugesu (Wiley-VCH, Weinheim, 2015).

[3] P. Santini, S. Carretta, G. Amoretti, R. Caciuffo, N. Magnani, and G. H. Lander, Multipolar interactions in f-electron systems: The paradigm of actinide dioxides, Rev. Mod. Phys. **81**, 807 (2009).

[4] M. J. P. Gingras and P. A. McClarty, Quantum spin ice: A search for gapless quantum spin liquids in pyrochlore magnets, Rep. Prog. Phys. **77**, 056501 (2014).

[5] W. Witczak-Krempa, G. Chen, Y. B. Kim, and L. Balents, Correlated quantum phenomena in the strong spin-orbit regime, Annu. Rev. Condens. Matter Phys. **5**, 57 (2014).

[6] A. Abragam and B. Bleaney, *Electron Paramagnetic Resonance of Transition Ions* (Clarendon Press, Oxford, 1970).

[7] R. J. Elliott and M. F. Thorpe, Orbital effects on exchange interactions, J. Appl. Phys. **39**, 802 (1968).

[8] F. Hartmann-Boutron, Interactions de superéchange en présence de dégénérescence orbitale et de couplage spin-orbite, J. Phys. (Paris) **29**, 212 (1968).

[9] R. Englman, *The Jahn-Teller Effect in Molecules and Crystals* (Wiley, London, 1972).

[10] I. B. Bersuker and V. Z. Polinger, *Vibronic Interactions in Molecules and Crystals* (Springer, Berlin, 1989).

[11] I. B. Bersuker, *The Jahn-Teller Effect* (Cambridge University Press, Cambridge, 2006).

[12] L. F. Chibotaru and L. Ungur, *Ab initio* calculation of anisotropic magnetic properties of complexes. I. Unique definition of pseudospin Hamiltonians and their derivation, J. Chem. Phys. **137**, 064112 (2012).

[13] L. F. Chibotaru, *Ab initio* methodology for pseudospin Hamiltonians of anisotropic magnetic complexes, Adv. Chem. Phys. **153**, 397 (2013).

[14] H. A. Jahn, Stability of polyatomic molecules in degenerate electronic states. II. Spin degeneracy, Proc. R. Soc. London, Ser. A **164**, 117 (1938).

[15] H. H. Claassen, G. L. Goodman, J. H. Holloway, and H. Selig, Raman spectra of MoF_6, TcF_6, ReF_6, UF_6, SF_6, SeF_6, and TeF_6 in the vapor state, J. Chem. Phys. **53**, 341 (1970).

[16] D. W. Osborne, F. Schreiner, K. Otto, J. G. Malm, and H. Selig, Heat capacity, entropy, and Gibbs energy of technetium hexafluoride between 2.23 and 350 K; magnetic anomaly at 3.12 K; mean β energy of ^{99}Tc, J. Chem. Phys. **68**, 1108 (1978).

[17] T. Sato, E. Lijnen, and A. Ceulemans, Jahn-Teller instability of icosahedral $[W@Au_{12}]^-$, J. Chem. Theory Comput. **10**, 613 (2014). The Γ_8 state also arises in icosahedral systems.

[18] W. Domcke, D. Opalka, and L. V. Poluyanov, Relativistic theory of the Jahn-Teller effect: p-orbitals in tetrahedral and trigonal systems, J. Chem. Phys. **144**, 124101 (2016).

[19] T. N. Morgan, Vibronic Coupling in Semiconductors: The Dynamic Jahn-Teller Effect, Phys. Rev. Lett. **24**, 887 (1970).

[20] J. E. Bray, Paramagnetic resonance of tetravalent neptunium-237 in single crystals of Cs_2ZrCl_6, Phys. Rev. B **18**, 2973 (1978). In the calculation of g factors, the excited Γ_8 state is used by mistake.

[21] E. R. Bernstein and L. W. Dennis, Electron-paramagnetic-resonance data interpretation for a $\Gamma_8(O_h)$ state in a cubic crystal field, Phys. Rev. B **20**, 870 (1979).

[22] N. Edelstein, W. Kolbe, and J. E. Bray, Electron paramagnetic resonance spectrum of the Γ_8 ground state of Np^{4+} diluted in Cs_2ZrCl_6, Phys. Rev. B **21**, 338 (1980).

[23] I. Halliday and J. W. Tucker, Jahn-Teller reduction factors and the spin-Hamiltonian parameters of $^4A_2$ (Γ_8) ground-state ions, J. Phys. C **21**, 5403 (1988).

[24] M. Karbowiak, J. Drożdżyński, S. Hubert, E. Simoni, and W. Stręk, Analysis of absorption and luminescence spectra of U^{3+} doped Cs_2NaYCl_6 and Cs_2LiYCl_6 single crystals, J. Chem. Phys. **108**, 10181 (1998).

[25] X. Zhou, C. S. K. Mak, P. A. Tanner, and M. D. Faucher, Spectroscopic properties and configuration interaction assisted crystal field analysis of Nd^{3+} in neat $Cs_2NaNdCl_6$, Phys. Rev. B **73**, 075113 (2006).

[26] A. S. Erickson, S. Misra, G. J. Miller, R. R. Gupta, Z. Schlesinger, W. A. Harrison, J. M. Kim, and I. R. Fisher, Ferromagnetism in the Mott Insulator Ba_2NaOsO_6, Phys. Rev. Lett. **99**, 016404 (2007).

[27] M. A. de Vries, A. C. Mclaughlin, and J.-W. G. Bos, Valence Bond Glass on an fcc Lattice in the Double Perovskite Ba_2YMoO_6, Phys. Rev. Lett. **104**, 177202 (2010).

[28] T. Aharen, J. E. Greedan, C. A. Bridges, A. A. Aczel, J. Rodriguez, G. MacDougall, G. M. Luke, T. Imai, V. K. Michaelis, S. Kroeker, H. Zhou, C. R. Wiebe, and L. M. D. Cranswick, Magnetic properties of the geometrically frustrated $S = \frac{1}{2}$ antiferromagnets, La_2LiMoO_6 and Ba_2YMoO_6, with the B-site ordered double perovskite structure: Evidence for a collective spin-singlet ground state, Phys. Rev. B **81**, 224409 (2010).

[29] C. A. Marjerrison, C. M. Thompson, G. Sala, D. D. Maharaj, E. Kermarrec, Y. Cai, A. M. Hallas, M. N. Wilson, T. J. S. Munsie, G. E. Granroth, R. Flacau, J. E. Greedan, B. D. Gaulin, and G. M. Luke, Cubic Re^{6+} ($5d^1$) Double Perovskites, Ba_2MgReO_6, Ba_2ZnReO_6, and $Ba_2Y_{2/3}ReO_6$: Magnetism, Heat capacity, μSR, and neutron scattering studies and comparison with theory, Inorg. Chem. **55**, 10701 (2016).

[30] C. H. Webster, L. M. Helme, A. T. Boothroyd, D. F. McMorrow, S. B. Wilkins, C. Detlefs, B. Detlefs, R. I. Bewley, and M. J. McKelvy, Influence of static Jahn-Teller distortion on the magnetic excitation spectrum of PrO_2: A synchrotron x-ray and neutron inelastic scattering study, Phys. Rev. B **76**, 134419 (2007).

[31] L. Ungur and L. F. Chibotaru, Computational Modelling of the Magnetic Properties of Lanthanide Compounds, in *Lanthanides and Actinides in Molecular Magnetism*, edited by R. Layfield and M. Murugesu (Wiley-VCH, Weinheim, 2015), p. 153.

[32] N. A. Bogdanov, V. M. Katukuri, J. Romhányi, V. Yushankhai, V. Kataev, B. Büchner, J. van den Brink, and L. Hozoi, Orbital reconstruction in nonpolar tetravalent transition-metal oxide layers, Nat. Commun. **6**, 7306 (2015).

[33] E. Lefrançois, A.-M. Pradipto, M. Moretti Sala, L. C. Chapon, V. Simonet, S. Picozzi, P. Lejay, S. Petit, and R. Ballou, Anisotropic interactions opposing magnetocrystalline anisotropy in Sr_3NiIrO_6, Phys. Rev. B **93**, 224401 (2016).

[34] L. F. Chibotaru, A. Ceulemans, and H. Bolvin, Unique Definition of the Zeeman-Splitting g Tensor of a Kramers Doublet, Phys. Rev. Lett. **101**, 033003 (2008).

[35] D. A. Varshalovich, A. N. Moskalev, and V. K. Khersonskii, *Quantum Theory of Angular Momentum* (World Scientific, Singapore, 1988).

[36] Although the total number of independent parameters describing the three operators μ_α is $10\times3=30$, in the case when the pseudospin $\tilde{S}$ is defined in a common Cartesian coordinate system, the g tensor pasteurizing the first-rank contribution to μ_α becomes a symmetric matrix imposing three constraints on three parameters.

[37] B. Bleaney, The spin hamiltonian of a Γ_8 quartet, Proc. Phys. Soc. London **73**, 939 (1959).

[38] W. Moffitt and W. Thorson, Vibronic states of octahedral complexes, Phys. Rev. **108**, 1251 (1957).

[39] G. F. Koster, J. O. Dimmock, R. G. Wheeler, and H. Statz, *Properties of the Thirty-Two Point Groups* (MIT Press, Cambridge, MA, 1963). The number $\sqrt{5/20}$ in the sixth row and the fifth column of Table 83 (p. 95) is replaced with $\sqrt{5/12}$.

[40] S. E. Apsel, C. C. Chancey, and M. C. M. O'Brien, Berry phase and the $\Gamma_8\otimes(\tau_2\oplus\epsilon)$ Jahn-Teller system, Phys. Rev. B **45**, 5251 (1992).

[41] F. Ham, C. H. Leung, and W. H. Kleiner, Relationships among Jahn-Teller reduction factors for a Γ_8 state in cubic symmetry, Solid State Commun. **18**, 757 (1976).

[42] M. C. M. O'Brien and D. R. Pooler, Reduction factors for dynamic Jahn-Teller systems in strong coupling, J. Phys. C **12**, 311 (1979).

[43] M. H. L. Pryce, Sign of g in Magnetic Resonance, and the Sign of the Quadrupole Moment of Np^{237}, Phys. Rev. Lett. **3**, 375 (1959).

[44] L. F. Chibotaru and L. Ungur, Negative g Factors, Berry Phases, and Magnetic Properties of Complexes, Phys. Rev. Lett. **109**, 246403 (2012).

[45] A. A. Granovsky, Extended multi-configuration quasi-degenerate perturbation theory: The new approach to multi-state multi-reference perturbation theory, J. Chem. Phys. **134**, 214113 (2011).

[46] T. Shiozaki, W. Győrffy, P. Celani, and H.-J. Werner, Extended multi-state complete active space second-order perturbation theory: Energy and nuclear gradients, J. Chem. Phys. **135**, 081106 (2011).

[47] F. Aquilante, J. Autschbach, R. K. Carlson, L. F. Chibotaru, M. G. Delcey, L. De Vico, I. F. Galván, N. Ferré, L. M. Frutos, L. Gagliardi, M. Garavelli, A. Giussani, C. E. Hoyer, G. Li Manni, H. Lischka, D. Ma, P.-Å. Malmqvist, T. Müller, A. Nenov, M. Olivucci, T. B. Pedersen, D. Peng, F. Plasser, B. Pritchard, M. Reiher, I. Rivalta, I. Schapiro, J. Segarra-Martí, M. Stenrup, D. G. Truhlar, L. Ungur, A. Valentini, S. Vancoillie, V. Veryazov, V. P. Vysotskiy, O. Weingart, F. Zapata, and R. Lindh, Molcas 8: New capabilities for multiconfigurational quantum chemical calculations across the periodic table, J. Comput. Chem. **37**, 506 (2016).

[48] Z. Barandiarán and L. Seijo, The *ab initio* model potential method. Cowan-Griffin relativistic core potentials and valence basis sets from Li ($Z=3$) to La ($Z=57$), Can. J. Chem. **70**, 409 (1992).

[49] See Supplemental Material at http://link.aps.org/supplemental/10.1103/PhysRevB.96.064416 for further information on AIMPs.

[50] Z. Barandiarán and L. Seijo, The *ab initio* model potential representation of the crystalline environment. Theoretical study of the local distortion on NaCl:Cu^+, J. Chem. Phys. **89**, 5739 (1988).

[51] J. L. Pascual, J. Schamps, Z. Barandiarán, and L. Seijo, Large anomalies due to insufficiency of Madelung embedding in *ab initio* calculations of $4f$-$5d$ and $4f$-$6s$ excitations of lanthanides in ionic crystals: The $BaF_2:Ce^{3+}$ crystal, Phys. Rev. B **74**, 104105 (2006).

[52] J. L. Pascual, Z. Barandiarán, and L. Seijo, *Ab initio* theoretical study of luminescence properties of Pr^{3+}-doped Lu_2O_3, Theor. Chem. Acc. **129**, 545 (2011).

[53] The atomic unit of the mass-weighted coordinate is $\sqrt{m_e}a_0$, where m_e is the electron mass and a_0 is the Bohr radius.

[54] K. D. Warren, Evidence for the Ham effect in bis-tetramethylammonium hexachloroneptunate(IV), Chem. Phys. Lett. **99**, 427 (1983).

[55] In Ref. [21], the eigenstates of μ_z with large and small eigenvalues are assigned to $|\tilde{S}\pm3/2\rangle$ and $|\tilde{S}\pm1/2\rangle$, which is different from our definition using group theory. Here, their g and G are recalculated based on our definition.

[56] D. G. Karraker and J. A. Stone, Mössbauer spectra and magnetic susceptibilities of Cs_2NpCl_6, $[(C_2H_5)_4N]_2NpCl_6$, and $[(CH_3)_4N]_2NpCl_6$, Phys. Rev. B **22**, 111 (1980).

[57] V. S. Mironov, L. F. Chibotaru, and A. Ceulemans, First-order phase transition in UO_2: The interplay of the $5f^2-5f^2$ superexchange interaction and Jahn-Teller effect, Adv. Quantum Chem. **44**, 599 (2003).

[58] M. Kotani, On the magnetic moment of complex ions. (I), J. Phys. Soc. Jpn. **4**, 293 (1949).